VHF–Interferometry and Radar Observation: Implications for Nitrogen Oxides Production

Nikolai Dotzek, Hartmut Höller

DLR – Institut für Physik der Atmosphäre, Oberpfaffenhofen

and

Claire Théry

ONERA – DMPH–EAG, Châtillon

Abstract. Results of a combined analysis of data from a C–band polarimetric Doppler radar and a 3D VHF interferometric lightning mapping system are presented. Using the 21 July 1998 EULINOX supercell thunderstorm, the lightning data weakly indicate the tendency for two preferred charge regions in the cloud, near the –15°C and the –30°C level. Also evidence is found for the presence of a lower positive charge center near the freezing level in some parts of the clouds. However, in zones of strong vertical motions these levels tend to give way to more three–dimensional domains of lightning activity. Therefore for a detection of any charge layers in vertical profiles averaging over too large regions in space and time is prohibitive. The correlation of VHF signals with radar reflectivity shows that in the growing storm peak activities are low and linked to reflectivities around 30 dBZ, while after the mature stage the largest activity is about three times higher and peaks at reflectivities of about 45 dBZ. A polarimetric hydrometeor classification indicates that most lightning activity occurrs where large graupel and small hail are present. A simple model based on scaling arguments provides a rough measure of flash length to be $L = 35 \pm 8$ km, and an estimate of global lightning–induced NO_X immission of $P(\mathrm{NO}) \simeq 10$ Tg(N) a^{-1}. The range of $P(\mathrm{NO})$ is $[2.9, 22]$ Tg(N) a^{-1}, and the EULINOX supercell storm alone produced 26 t(N) within a two hour period.

1. Introduction and Objectives

The two–year European lightning NO_X (LNO_X) project (EULINOX) aimed at an improved understanding of the processes of NO_X production $P(\mathrm{NO})$ within central European thunderstorms. The main goal was to obtain a more reliable estimation of the global NO_X production due to lightning discharges compared to man–made and other natural sources, such as fuel combustion in ground- and air traffic, industry or in–soil nitrogen fixation by bacteriae.

During the EULINOX project a great variety of analysis methods were applied: aircraft measurements of chemical constituents within and around thunderclouds uncovered extremely high mixing ratios of NO in cumulonimbus (Cb) anvils (Huntrieser et al., 2000).

Interferometric measurements of VHF sources from lightning discharges in two and three dimensions were made by the ONERA (Théry et al., 2000) and compared to the two–dimensional LPATS system (Théry, 2000). Furthermore, the C–band polarimetric Doppler radar at DLR in Oberpfaffenhofen also provided three–dimensional information on the storm structure and allowed for an identification of the different hydrometeor types in the thundercloud and the accompanying anvil region. Therefore the combination of data from ONERA's VHF interferometric lightning mapper (ITF) and DLR's polarization diversity radar could be expected to provide a detailed view on the evolution of the lightning activity in space and time. A special focus was on the cloud microphysical processes which enable or enhance the charge separation mechanisms inside a cumulonimbus cloud.

The main objectives of this twofold approach to the cloud electrification problem were:

- identification of the main regions or levels of lightning activity inside the cloud and comparison to theoretical predictions,
- quantification of the spatial extent of single flashes, and clarification of how lightning activity was distributed and oriented spatially inside the cloud: where there are horizontal layers in the cloud and where vertical or oblique regions with lightning discharges can be found,
- identification of correlation between lightning discharges and certain hydrometeor types or other radar parameters, such as the reflectivity factor Z,
- quantification of any temporal trend in these correlations due to the evolution of the thundercloud.

Most of these objectives are directly linked to the NO_X production. If intracloud (IC) and cloud–to–ground (CG) flashes have a different potential to produce NO_X, it will also be necessary to know the percentage of IC or CG flashes within a certain period of time or for a whole thunderstorm. This topic is addressed in detail by Théry (2000, this volume). The spatial extent is needed for any estimate of $P(\mathrm{NO})$ that involves total flash lengths L or the production per unit length, such as the approach presented by Stith et al. (1999). The last two objectives will be useful to develop improved or new parameterizations of LNO_X in mesoscale and global models (cf. also Fehr, 2000b, this volume) compared to existing methods (Price & Rind, 1992, 1993).

2. Work Performed

The data evaluation focused on the supercell storm of 21 July 1998 (Höller et al., 2000). This storm was the right–mover of a storm splitting at about 16:45 UTC over the Allgäu region in southern Germany. While the left–moving cells decayed very soon, the other cell heading in an easterly direction within the mid–level flow from SW intensified very rapidly and developed supercell characteristics such as a single persistent updraft, a bounded weak echo region, the echo overhang and mid–level mesocyclonic rotation. Hail was reported, but no severe damage was observed.

After 17:00 UTC the young supercell storm approached the measuring area around Oberpfaffenhofen (OP). The onset of lightning activity was monitored both by the LPATS system and the two ITF stations Oberschleißheim (OS) and Wielenbach (WB) operated by ONERA. The southern station (WB) was equipped with the 3D–sensor allowing for a

three–dimensional reconstruction of the location of lightning–induced VHF emissions near 114 MHz. During its evolution, the supercell passed over the 3D station between 18:00–18:15 UTC, already beginning to decay. The most noticeable cloud growth and internal organization took place between 17:30 UTC and 18:00 UTC. The storm was tracked by radar and observed with sector volume scans and additional two–dimensional scans, such as range–height indicator (RHI) and plan position indicator (PPI) displays.

The ONERA provided their lightning data in two basic formats: i) volume data, ii) point data. The volume data consisted of information on the number of VHF sources which occurred during 3 min time intervals within a volume of 1 km^3. These volume elements or voxels were spatially centered at the nodes of the cartesian grid shown in Fig. 1. The point data on the other hand directly provided the 3D reconstruction of single lightning flashes. Using algorithms exploiting spatial and temporal information about the VHF sources as well as the shape of the signal in ONERA's raw data, separate flashes were identified (Théry et al., 2000).

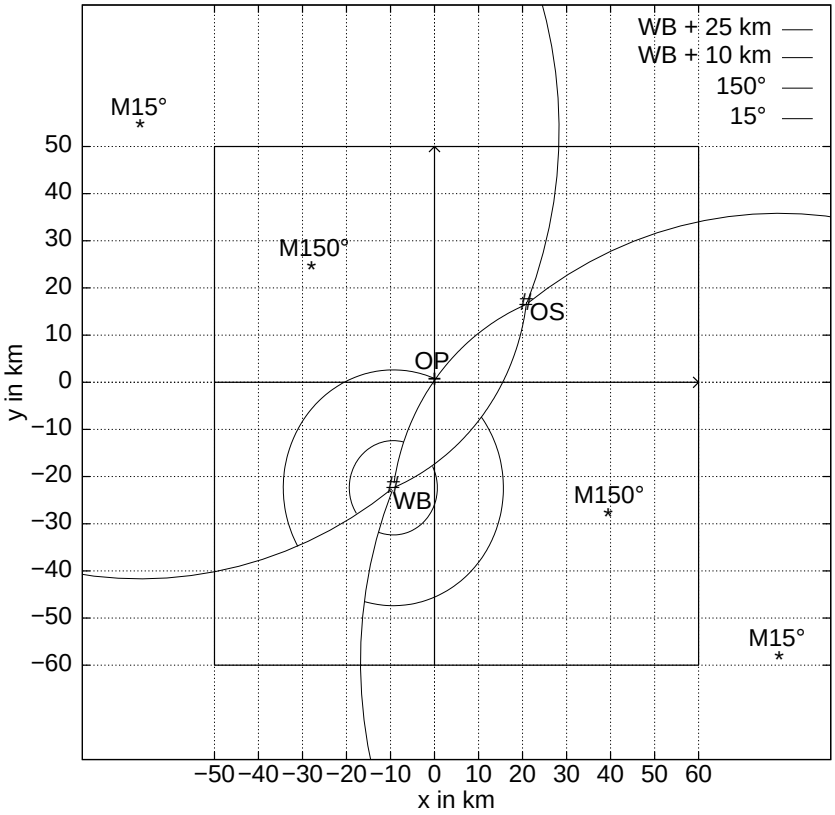

Figure 1. Evaluation area around Oberpfaffenhofen (OP). The DLR radar is located in the origin. Of the two ITF sites (OS, WB), the southern station at Wielenbach was the 3D sensor. The 1 km^3 grid extent is shown by the square outline. Note the two ring segments around WB.

So to facilitate the 3D analysis and the comparison to the ITF volume data, from the archived raw data the Doppler radar volume scans were interpolated to the same cartesian 110 × 110 × 15 grid with a mesh spacing of 1 × 1 × 1 km^3. In addition the fields interpolated on this grid could be further processed with a 3D visualization software package which enabled a simultaneous look at radar, ITF, LPATS and aircraft data.

The horizontal grid extent is shown by the solid square boundary in Fig. 1 with OP located in the origin. In the vertical the grid extended up to 15 km AGL, while the highest radar echo tops of the supercell were found in 13–14 km AGL. Fig. 1 also gives the location of the two ITF sensors and an example of the boundaries of the ITF lobes to the NW and SE of Oberpfaffenhofen in which flashes could be detected. Cf. Théry et al. (2000, this volume) for a detailed description of these lobes.

In the ring–like region shown in Fig. 1 around Wielenbach the whole main part of the EULINOX supercell cloud from below the freezing level near 3.5–4 km AGL to the upper

region of the Cb was simultaneously visible for the ITF. Such a complete view of the bulk volume of a cumulonimbus is highly desirable when the vertical structure of lightning activity as a whole is to be studied. For this reason the two segments of the range ring around the ITF 3D station in Wielenbach were selected as the main evaluation areas of the VHF lightning data. Unless otherwise stated the ITF volume data were considered at grid points within these ring segments and a single flash from the ITF point data was used for analysis if the centroid of the flash fell into one of these ring segments, leading to a total of 2280 single flashes for the available time period from 14:00 to 22:00 UTC on 21 July 1998.

To evaluate radar and ITF data, the following work was performed: the radar data was used to analyze storm evolution and dynamics during the whole life cycle of the supercell. Furthermore, the hydrometeor classification scheme developed by Höller et al. (1994) and Höller (1995) was applied to identify the location of different hydrometeor classes and to quantify their mixing ratios. The ITF point and volume data were also plotted into the radar pictures to find preferred locations of VHF signals with respect to up- or downdraft structure or to hydrometeors such as graupel particels which are expected to contribute to the in–cloud charge separation (Williams, 1989; Saunders, 1993; MacGorman & Rust, 1998). Correlations between lightning activity and various radar parameters have been analyzed to shed light on the most suitable mesoscale model parameters for an improved lightning parameterization. From the ITF information alone mean vertical profiles of VHF activity have been computed to test the data against current theoretical models indicating the existence of distinct peak levels of VHF activity. For the detection of these peaks an algorithm especially adapted to the data structure was developed. Graphical examination of single flashes derived from the point data was further used to find an average horizontal and vertical extent of the flashes and to trace the electrical activity of the storm through the time span from 17:00 to 19:00 UTC. In this way a detailed picture of the electrical and microphysical behaviour of the observed Cb–cloud could be gained and is presented in the following sections.

3. Results

Some introductory remarks on the current knowledge of the lightning discharge are necessary for an understanding and interpretation of the results. Fig. 2 summarizes the key features by depicting the situation for negative (CG–) and positive (CG+) cloud–to–ground as well as intracloud lightning (IC) within an idealized cylindrical Cb–cloud extending from below the freezing level up to the tropopause region. The mean diameter of the cloud is D while the altitude intervals traversed by the flashes from cloud to ground or within the cloud are H_-, H_+, and H respectively.

Both theoretical (Williams, 1989; Saunders, 1993) and also experimental results (Rison et al., 1999; Solomon et al., 1999) indicate a negative charge center around the $T = -15 \pm 10$°C level and an upper positive charge center near the $T = -30 \pm 10$°C level. A smaller lower positive charge region can sometimes be found close to the freezing level (Williams, 1989). These three levels are schematically indicated in Fig. 2 with a), b), and c). This figure will also be used later on for model parameterization purposes.

To incorporate this tripole model in the synoptic setting of 21 July 1998 we have to assess the heights of the three temperature levels. As can be deduced from the composite afternoon vertical sounding (Fehr, 2000a), temperatures near the ground level ranged

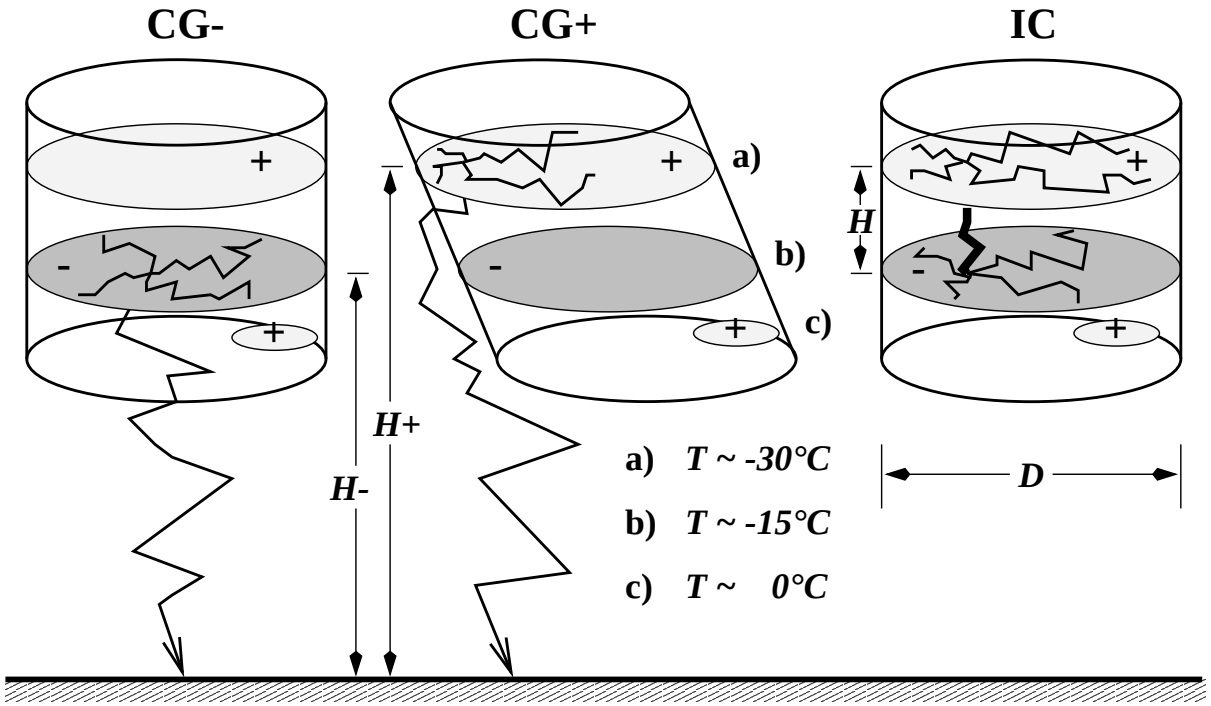

Figure 2. Conceptual tripole–type model of different lightning types and related temperature levels of the three main charge layers (cf. Williams, 1989; Houze, 1993, p. 282).

between 25°C and 30°C. The height of the negative charge center can be expected to be within a range from 4.5 to 7.5 km AGL, and the upper positive charge center approximately 3 km higher up, i. e. at a height of about 7.5 to 10.5 km AGL.

3.1. Vertical Profiles of VHF Activity

Within the ring–shaped area around the 3D ITF station Wielenbach shown in Fig. 1 the vertical profiles of VHF sources integrated over 3 min intervals and given on the 1 km^3 grid have been analyzed for the presence of peak levels. These may give an indication for the existence of the charge centers predicted by theory. To find only distinct peaks in the vertical VHF profile at a given grid point i) the profile as a whole must not be sparse, i. e. the total number of VHF sources in the profile exceeds the number of vertical grid points, ii) the number of VHF sources at the peak level must exceed 15 % of the total number of VHF sources in the profile, iii) the vertical distance between consecutive peaks must exceed the vertical grid spacing to assure that plateaus in the profiles are not classified as two sparate peaks.

At most grid points with distinct peaks in the vertical profiles, there was only one maximum (666 cases), in another 204 cases two peaks were found, and in only 24 cases three maxima were detected by the algorithm. However, the vast majority of vertical profiles does not show any distinct maximum of VHF activity, mostly due to the already mentioned sparseness of the profiles.

Averaging all VHF profiles within the ring around Wielenbach only yielded one maximum of VHF activity located at 3.5 km AGL, i. e. near the freezing level. Any upper level maximum, if present, was smeared out by the averaging process. However, as theory predicts clearly distinguishable charge layers at least in certain parts of a thundercloud

we could expect e. g. that at most grid points with two peaks in the vertical profile of VHF sources these peaks are located at similar altitude levels. In addition profiles with one peak should also reproduce one of the predicted charge layers and therefore coincide with one of the peak levels in multi–peak VHF profiles. To test this hypothesis the vertical profiles were averaged in a different way: those with one peak and two peaks were averaged separately.

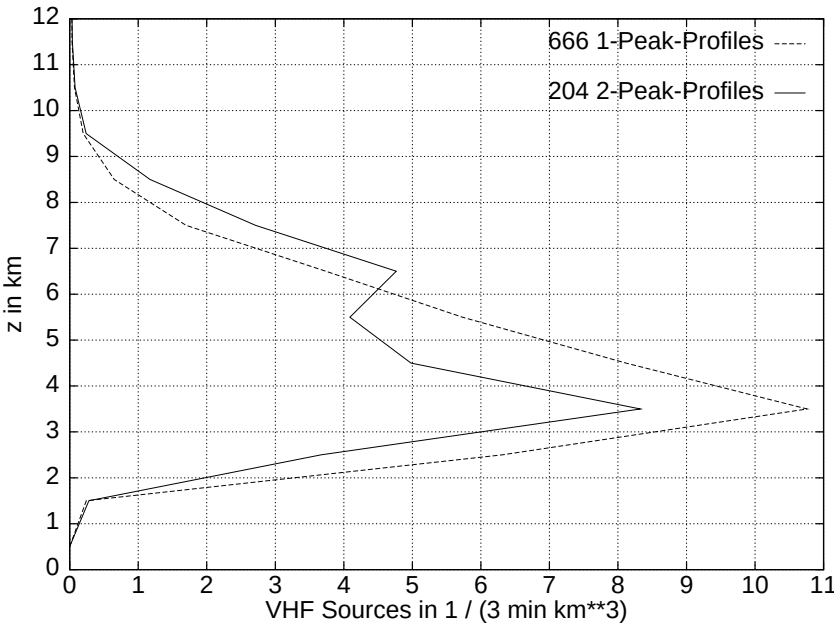

Figure 3. Average (17:00–20:00 UTC) vertical profiles of those 666 VHF columns containing only one distinct maximum (dashed) and those 204 VHF columns containing two distinct maxima (solid).

The result of this separate averaging is depicted in Fig. 3. The dashed line gives the average of all 1–peak profiles and the solid line the average of the 2–peak profiles. In both cases the low–level maximum at 3.5 km AGL is most pronounced. The solid curve, however, shows a secondary maximum at 6.5 km AGL which corresponds to the –15°C level of 21 July 1998. Yet in neither of the average profiles do we find an upper–level maximum near the –30°C region inside the cloud. Instead the peak near the freezing level dominates all profiles (even an average of all sparse profiles without distinct peaks leads to a flat maximum at that level).

To find a possible reason for this result, it is necessary to consider the VHF emission characteristics of the various flash components (cf. Théry, 2000; Théry et al., 2000) inside the Cb–cloud. One should also take into account that e. g. VHF emissions of negative leaders appear to be pressure–dependent: higher pressure levels can lead to a larger number N_{VHF} of VHF signals (Lalande & Bondiou–Clergerie, 1997). So aside from possible VHF amplitude variations, we might argue that such a pressure–dependence or an unusually large number of low–level negative leaders (Théry et al., 2000) in the EULINOX storm could be the source of the dominant low–altitude peak in the mean VHF profiles.

In this context, separately averaging the 1–peak and 2–peak profiles was a suitable aid to check consistency here: we had to expect one of the maxima at the same altitude in both mean profiles. The secondary peak at 6.5 km AGL could then only be detected by separate averaging. However, at most other grid points the situation is not that definite, indicating that the tripole model (cf. Williams, 1989, and Fig. 2) cannot account for all details of thunderstorm electrification (Rust & Marshall, 1996). Therefore even the weaker secondary maximum noticeable in Fig. 3 is no longer visible in an average over all vertical profiles.

3.2. Characteristics of Single Flashes

To clarify this first impression of the vertical distribution of VHF activity gained by analysis of the volume data, now the reconstructed location of VHF sources in 3D (point data) will be considered. The Figs. 4 and 5 provide quite different examples of IC flashes. The large square in the figures presents the x,y–projection of the VHF sources combined with the dash–dotted outline of the ITF–lobes. Similar projections to the vertical x,z- and y,z–planes are shown as well and also depict the 8° and 42° elevation limits (Defer, 1999) of the ITF sensor (dashed lines). The small diagram in the upper right corner gives the vertical distribution and total number of VHF sources for the flash.

Looking first at an IC lightning with a dominant negative leader in Fig. 4, a strong maximum of VHF activity can be seen near the 3 km AGL level: we observe a dense cloud of points in the lowest parts of the discharge. These belong to the negative leader phase.

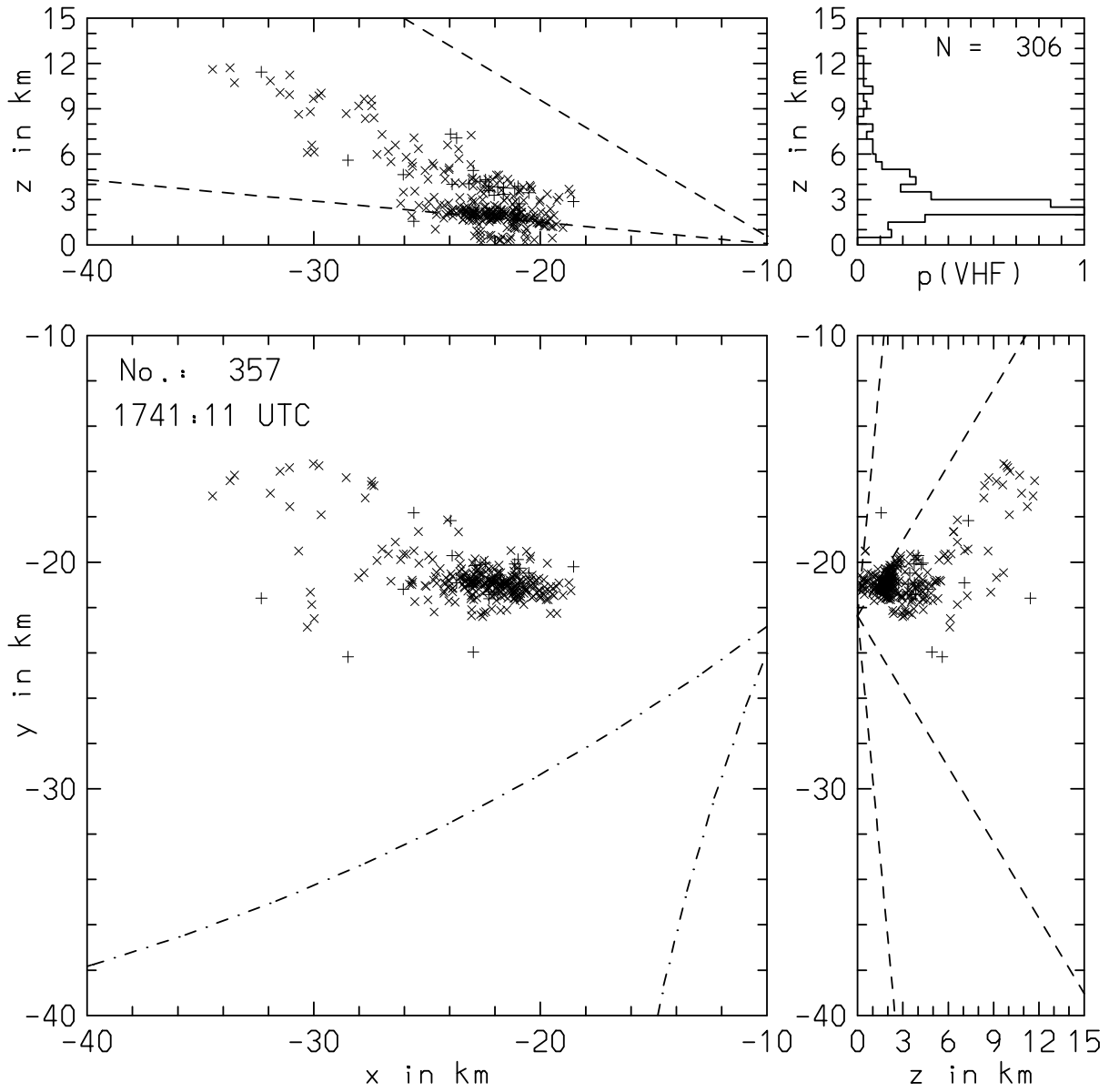

Figure 4. An example of an IC flash with a dominant low–level negative leader. Each plotted symbol corresponds to one VHF source.

As mentioned above, low–level negative leaders may have the potential to be very active in VHF due to the higher air pressure compared to upper tropospheric regions (Lalande & Bondiou–Clergerie, 1997). Above 7 km AGL there is only little VHF activity accompanied with recoil streamers in this flash. Especially the y,z–section shows a dense cloud of VHF signals below 5 km AGL and a region of more horizontally widespread VHF activity above 5 km AGL in the region where we would expect the negative charge center. However, some few VHF signals are found above 9 km AGL as well and indicate upper–level discharges inside the fast–growing supercell cloud. This is a more exceptional case of the schematic model in Fig. 2 for an IC flash. A dominant low–level negative leader connecting to Cb mid–levels presents the "lower branch" of the tripole model.

The impression that low–level negative leaders are so prominent in the data is an interesting peculiarity of the 21 July 1998 EULINOX storm. In general one would expect

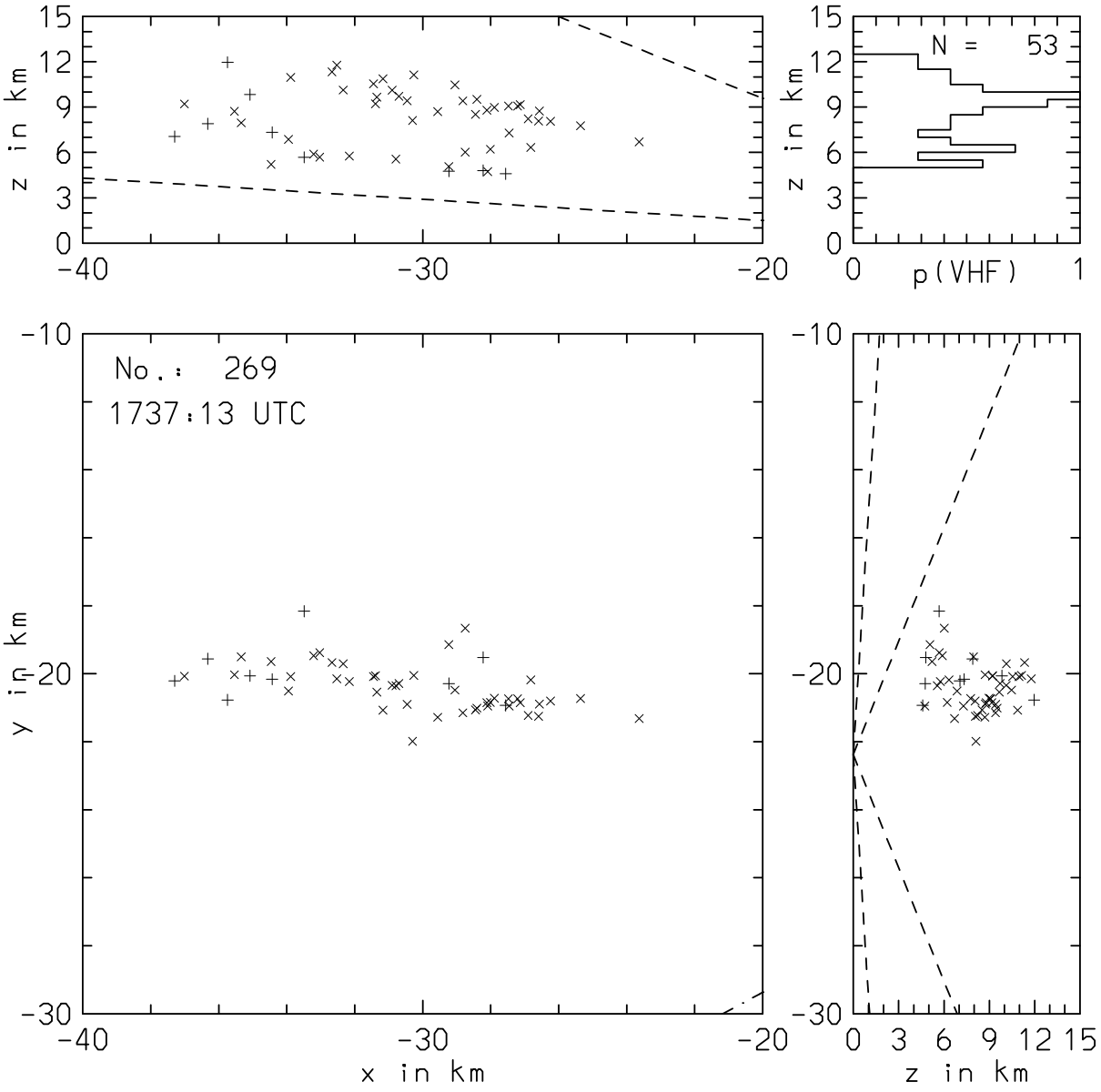

Figure 5. As Fig. 4, but for a high–altitude IC flash. Two horizontally oriented regions of VHF activity near 6.5 km and 9.5 km AGL become visible (cf. Fig. 2).

that most negative leaders propagate within the upper–level positive charge layer. In this particular supercell, at least for certain regions and time periods, the lower positive charge region appears to have been enhanced by a special dynamical and microphysical setting (Williams, 1989).

The intracloud flash shown in Fig. 5 having occurred 4 min before the IC flash of Fig. 4 gives a very instructive impression of the IC activity of this EULINOX storm. This flash, as many others, comes very close to the basic perception of intracloud lightning presented in Fig. 2 and MacGorman & Rust (1998, p. 203) as well as other measurements (Shao & Krehbiel, 1996; Defer, 1999; Rison et al., 1999; Solomon et al., 1999; Stith et al., 1999). The distribution of VHF sources in the vertical shows two distinct maxima at about 6.5 km and 9 km AGL. The upper peak is even more prominent than the lower one. Both levels which correspond to about the –30°C- and the –15°C altitudes, appear to be connected vertically in a region near $(x, y) \simeq (-27, -21)$ km off the radar at Oberpfaffenhofen. While the lower VHF region shows little vertical variation from one end of the flash to the other, the layer of upper–level VHF activity gradually rises from 8 km at the eastern edge to 11 km AGL at $x \simeq -32$ km before it descends again to about 8 km at the western end of the IC lightning. However, some care has to be taken because near the western end of the flash the points from the upper and the lower level come very close to each other. So a clear distinction between the two levels is no longer possible in this region.

Nevertheless this mentioned rise and fall of the upper cloud of VHF sources is in satisfactory agreement with the approximate location of the updraft core within the strongly developing supercell at that time. The location of the greatest altitude in this flash is close to the downshear edge of the updraft while the edges of the flash are located farther away from the updraft core near $(x, y) \simeq (-32, -28)$ km. As pointed out by Stolzenburg & Marshall (1998) and Williams (1989, cf. Fig. 3 therein), the upper positive charge layer can be more easily affected by the storm's dynamics and can therefore show larger variations in altitude throughout the Cb–cloud. The negatively charged region around the –15°C level, however, remains less affected by such changes in the updraft strength. In this region near the Cb–cell's main updraft the phenomenon might be interpreted in the following way: charge separation leads to positively charged small ice crystals in the upper part of the cloud and negatively charged larger hydrometeors at intermediate levels. Due to their small terminal velocity, the floating ice crystals higher up can respond to variations in vertical air motions much easier compared to the larger particles beneath (Williams, 1989). Furthermore the slowly falling ice crystals can be advected at nearly constant altitude by the horizontal wind even without supporting updrafts, while larger particles floating beneath for longer time periods require a distinct range of updraft speeds. This might serve as a possible explanation for the impression from Fig. 5 that the upper region of VHF sources is more horizontally widespread and more continuous than the lower one.

What can also be observed in the figure is the small total number of 53 VHF signals for this high–altitude IC flash. The points in this case stem from recoil streamers being fast and short duration discharges compared to the leader phase (Théry et al., 2000). Similar to the IC discharge shown in Fig. 4 the small amount of points will lead to a small influence of upper–level VHF sources when average vertical profiles over many separate lightning events are computed. Aside from the fact that the levels of peak VHF activity in general show a considerable variation in time and space, this is especially so for the upper–level positive charge region varying strongly with updraft intensity and hosting only relatively few VHF signals. This again points at a probable reason why no upper level maximum in

the average vertical VHF profiles could be found in the preceding section. To identify any upper positive charge region one should focus on shorter time periods and smaller regions in space, as done in this section.

3.3. Microphysics Revealed by Radar

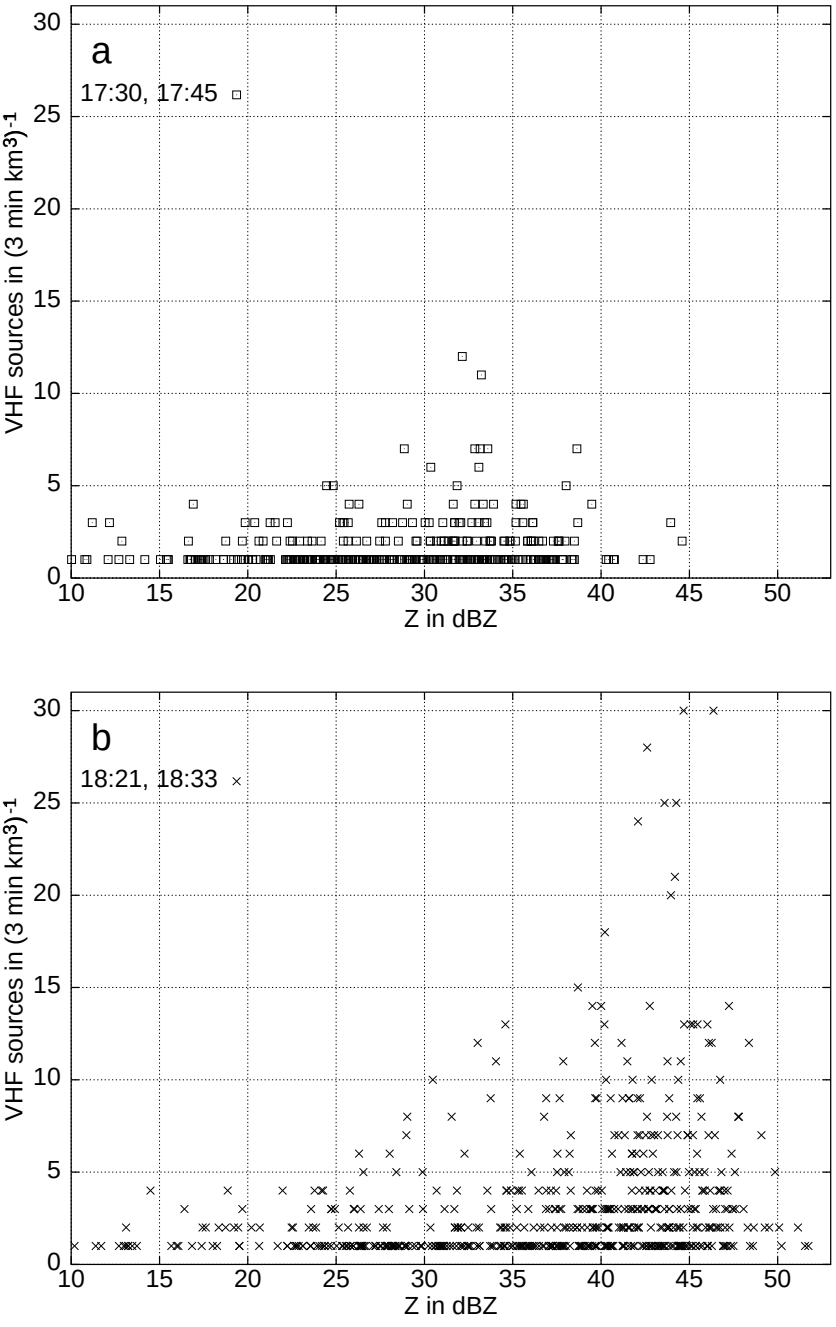

Figure 6. Scatter plot between number of VHF sources per 3 min interval km^{-3} and radar reflectivity factor Z. At 17:30, 17:45 UTC (a, squares) the data show a modal value of about 32 dBZ and weak skewness. The 18:21, 18:33 UTC data (b, crosses) are strongly skewed with a peak at about 45 dBZ.

After evaluation of the VHF interferometer results in the sections before we now incorporate the C–band polarimetric Doppler radar measurements. This will yield valuable information on the coupling between cloud microphysics and lightning discharges necessary for developing parameterizations for mesoscale or global models. Aside from the vertical profile of VHF activity studied before, modellers need to relate the flash location and -rate to prognostic variables of their models, or quantities derived of these variables (Fehr, 2000a). One of these derived quantities is the radar reflectivity factor Z being a function of hydrometeor content. The radar reflectivity factor can easily be computed from the output of mesoscale cloud models (Houze, 1993) so it would be highly desirable to find clear relations between lightning activity and reflectivity factor.

In this context the analysis again yielded instructive results. Often the region of most VHF activity was shifted away

from the reflectivity core of the supercell storm. The shift was mostly to the left downshear side of the storm's center, i. e. on the northern flank of the east–moving storm. To obtain information on the correlation between number of VHF sources N_{VHF} and reflectivity factor Z, the volume data measured by the radar at 17:30, 17:45, 17:57, 18:09, 18:21, and 18:33 UTC were related to the ITF volume data giving the sum of VHF sources within 3 min starting at the six given times of the radar volume scans. As the radar data was interpolated onto the same 1 km^3 grid as used for the ITF data, the points could directly be analyzed with a scatter plot of N_{VHF} versus Z.

This is shown in Fig. 6 a for the growing phase of the storm (17:30, 17:45, squares) and in Fig. 6 b for its decaying stage (18:21, 18:33, crosses). In all four volume scans the highest observed reflectivities were in the range from 50 to 52.5 dBZ. In the developing stage of the storm, no VHF data points are found for Z $\gtrsim$ 43 dBZ. Instead, weak VHF activity is found with usually less than 10 VHF sources per 3 min interval and per km^3. The peak of the scattered points is located at roughly 32 dBZ dropping towards higher values of Z and a slower decrease towards lower reflectivity factors. This skewness towards the higher values of Z is also found during the decaying stage of the storm. But quantitatively the differences are large: the reflectivity data now extend up to about 52 dBZ and the VHF activity also has increased substantially: many voxels have 10 or more sources per 3 min interval and per km^3 with a peak value of 30. In addition the location of this maximum has shifted towards higher reflectivity factors. Instead of 32 dBZ in the early stage, the scatter plot now peaks at 45 dBZ and then drops off very rapidly with increasing Z. The data are now more strongly skewed than before, but in general the shapes of the two scatter–data sets seem to bear a similarity, because the data region of Fig. 6 a coincides with the left flank of that in Fig. 6 b.

Table 1. Hydrometeor classification scheme.

Index	Hydrometeor Type
0	Thin cloud (no classification)
1	Small raindrops
2	Rain
3	Small graupel, snow
4	Large graupel (dry), small hail (dry)
5	Rain, small hail (wet)
6	Hail (dry)
7	Hail (wet)
8	Large hail (porous, wet)
9	Large hail (wet)
10	Rain and large hail (wet)
11	Rain and hail

To identify which hydrometeors were responsible for these findings, the hydrometeor classification scheme developed by Höller et al. (1994) and Höller (1995) was used to compute the dominant hydrometeor types in the radar's scan volume from the polarimetric radar data Z, ZDR, LDR. The classes of the Höller scheme are summarized in Tab. 1. The best candidates for a high correlation with lightning discharges are, according to theory, graupel, hail, and ice crystals or snow.

Fig. 7 was computed from the radar volume scan and the VHF volume data on the 1 km^3 cartesian grid at 17:57 UTC close to the stage of maturity of the EULINOX supercell storm of 21 July 1998. The color code is given for the values of Tab. 1 and the diagram shows three sections through the radar volume: a constant–altitude PPI (CAPPI) and two RHIs in x,z- and y,z–planes, respectively. The location of the sections is given by the orange solid lines in the figure. One can draw the conclusion from this diagram that the VHF activity is mainly linked to large graupel and small hail. Similar pictures from the other available radar volume data (not shown here) support this observation.

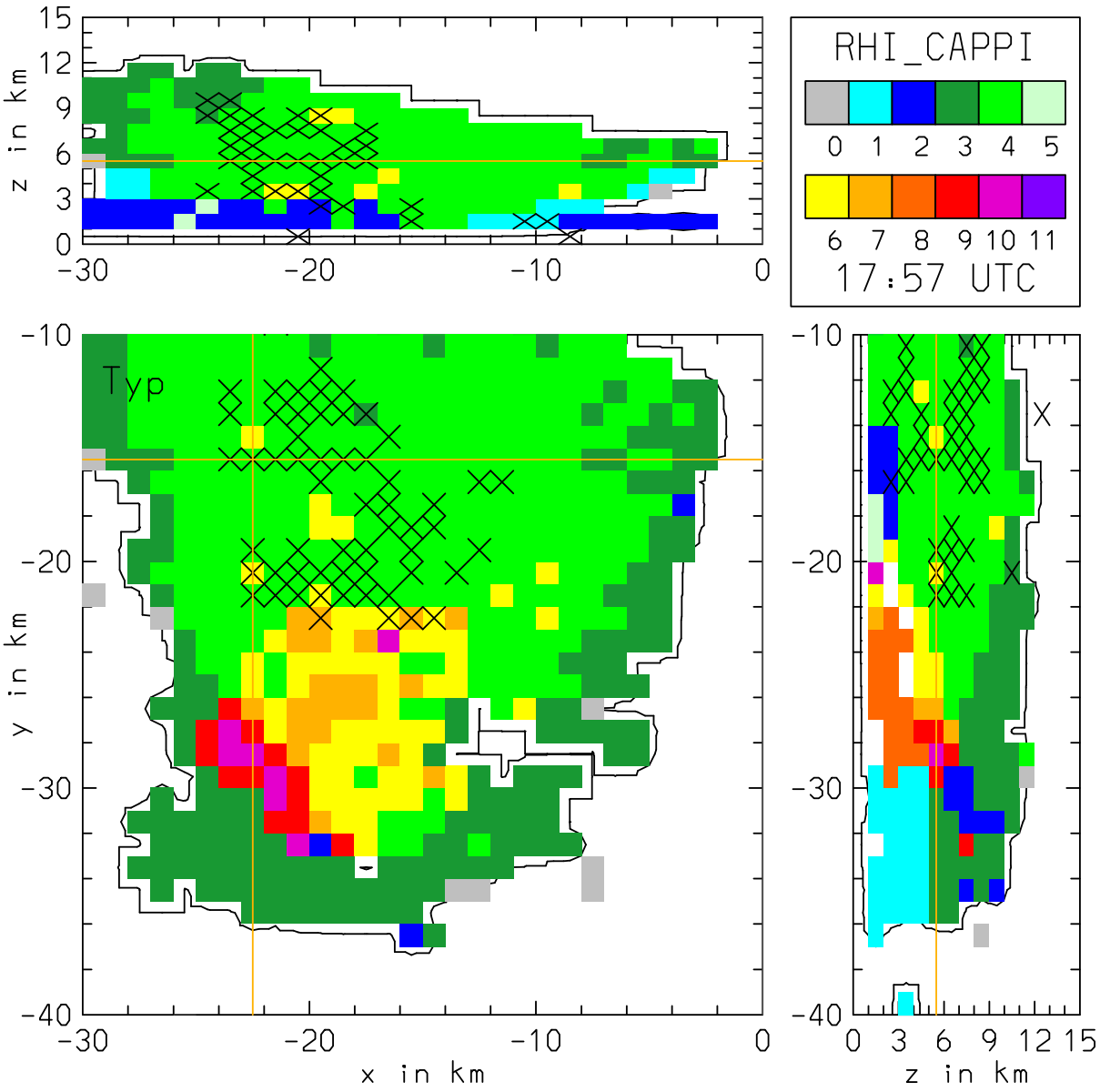

Figure 7. Analysis of the hydrometeor field according to Tab. 1 for a horizontal section (CAPPI) and two vertical sections (RHI) through the storm at 17:57 UTC. The location of the sections is depicted by the thin orange lines. VHF activity between 17:57 and 18:00 UTC is marked by the black crosses (×). The regions 3–6, i. e. large graupel and small hail are favorable to lightning discharges.

The vertical sections seem to indicate some tendency for horizontal layering of VHF activity near 3.5 km, 6 km, and 9 km AGL (cf. especially the x,z–section). But it is also apparent that this structure is only established in certain regions of the cloud. The tripole model presented in Fig. 2 cannot be expected to be valid everywhere inside the cloud. It is plausible that in regions of very strong up- and downdrafts such as the storm's core at (–18, –30) km, no VHF signals are observed. Here in the region of hailstone growth the riming graupel mechanism likely to be involved with charged cloud layers in not in effect.

Focusing on the graupel region inside the storm, another RHI scan offers a closer look at the vertical structure of the lightning discharges (Höller et al., 1999b, 2000, this

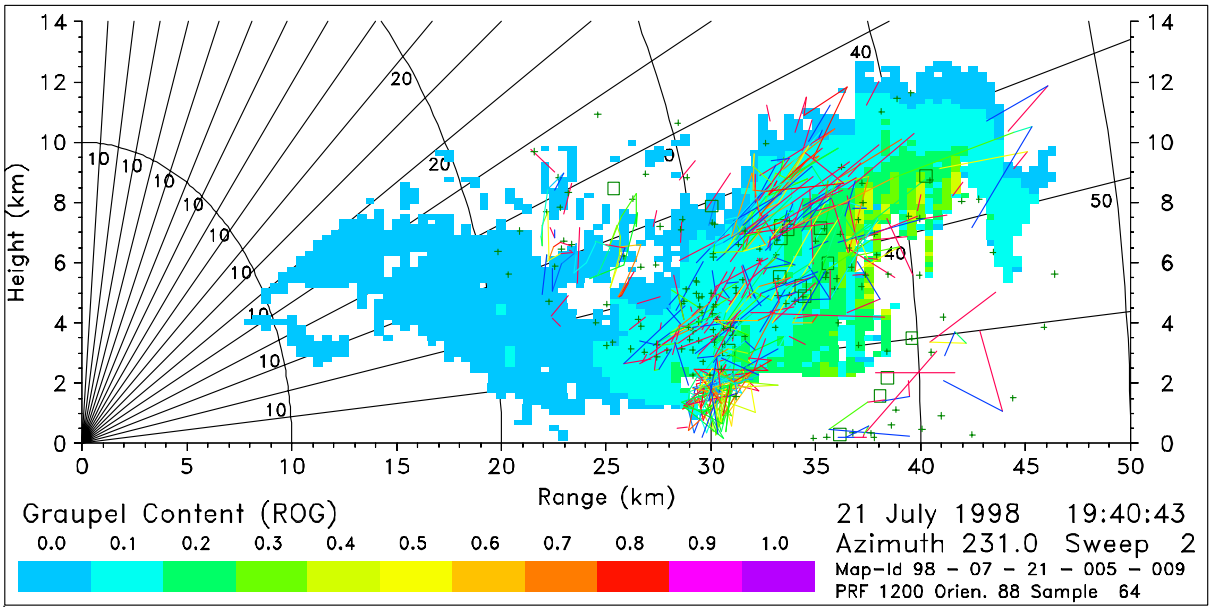

Figure 8. RHI at 231° azimuth showing the graupel content in $g\,m^{-3}$ at 17:40 UTC. Nearby discharges having occurred within ±30 s and ±10° azimuth (colored line segments) are mostly located within the graupel region downshear of the supercell updraft core (cf. MacGorman & Rust, 1998, p. 52).

volume). Fig. 8 is a range–height section at 231° azimuth from OP at 17:40 UTC, when the supercell was still developing. Here only the graupel content in $g\,m^{-3}$ is shown together with nearby VHF signals (colored line segments and crosses) occurring within a ±30 s time- and ±10° azimuth window around the RHI scan at 17:40 UTC. Again the majority of VHF sources is found in the graupel zone, few signals stem from the hail core (to the right of the graupel region) and the snow region in the anvil (to the upper left of the graupel field). However, in this case no horizontal layering of the lightning discharges can reliably be diagnosed. Instead the VHF sources group vertically among the graupel particles, leading to this waterfall–like structure on the downshear side of the east–moving updraft core.

So the impression gained from the combination of radar and ITF data remains ambiguous. While for certain regions of the cloud some evidence in favor of the tripole model of thunderstorms can be inferred, this is not so for other regions, e. g. in the vicinity of strong vertical motions.

3.4. Model Estimate of LNO_X Production

One of the main goals of the EULINOX project was to improve the understanding and current quantitative estimates of NO_X production on both the local and the global scale. As proposed recently (Gallardo & Cooray, 1996) and supported by both the LINOX (Höller et al., 1999a) and EULINOX in–cloud chemical measurements (Huntrieser et al., 2000, this volume), IC flashes are likely to be about as effective in producing NO_X as CG flashes. Here the information gathered by ONERA's ITF system for the supercell storm of 21 July 1998 showed the large percentage of intracloud lightning for that storm (Théry, 2000). From their detailed analysis of the ITF data, Théry et al. (2000, this volume) found a mean value for flash length in the EULINOX storm of about 30 km, a local production

P(NO) of 80 t(N) within eight hours of storm activity and a global estimate for P(NO) of 22 Tg(N) a^{-1}.

In the context of the present paper we will pursue a different objective and make a step towards modified parameterizations of lightning discharges for mesoscale models. Similar to Fehr (2000a,b) we will try to find an approach which is both simple and applicable to reproduce the gross features of NO_X production in thunderstorms. In contrast to the approach of Price & Rind (1992, 1993) we will proceed by trying to synthesize radar and ITF information in order to develop a simple conceptual model of NO_X production by lightning discharges. A preliminary evaluation of this model will be performed by estimating both local and global LNO_X production. For the latter we propose a global average thundercloud (for which we use the smaller Cb–cells of 21 July 1998 as prototypes) with an assumed fixed mean flash length while for the former we will discriminate between different flash types of the EULINOX supercell and use values for the mean flash rate and the relative contribution from each flash type from Théry (2000).

Table 2. Geometric parameters contributing to an estimate of flash lengths (cf. Fig. 2). Additional values for the special case of the EULINOX supercell storm are also given.

Flash	H_{EULINOX} km	D_{Model} km	L_{Model} km	D_{EULINOX} km	L_{EULINOX} km
CG-	6.5	10	16.5	20.0	26.5
CG+	9.5	10	19.5	20.0	29.5
IC	3.0	10	23.0	20.0	43.0

We will tackle the problem to derive the necessary measure of the spatial flash extent from the standpoint of scale analysis and a conceptual model derived from Fig. 2. The basic assumptions of this model are: first that the horizontal scale of a flash propagating within one of the main charge layers is of the order of the Cb–cell diameter D, second that the vertical scale of a flash is the height of the involved charge region above ground level (i. e. H_- and H_+ for CG flashes) or the height interval between the main charge layers (for an IC flash). As intracloud discharges according to our simple model encompass twice the cloud diameter due to their propagation within both charge layers, they will have the greatest flash lengths in the majority of cases.

As summarized in Tab. 2 meteorological scale analysis usually assumes both horizontal and vertical dimensions of a Cb–cloud to be 10 km. This was also the typical diameter of the smaller cumulonimbus clouds occurring on 21 July 1998. However, the observed diameter of the EULINOX supercell storm of this day as determined by the maximum horizontal dimension of the Z > 30 dBZ core, was about a factor of two larger, leading to $D_{\mathrm{EULINOX}} = 20$ km. The threshold value of 30 dBZ was chosen here to separate the convective storm center from its more stratiform outer regions. As the anvil region of the supercell was still connected with the mentioned smaller storms to the north, a lower threshold would not have given a unique criterion to define isolated closed cells. For the altitude levels of the main charge regions we only apply the EULINOX values also given in Tab. 2. From the conceptual model as introduced above we now find:

$$\begin{aligned} L_{\mathrm{CG-}} &\simeq H_- + D \\ L_{\mathrm{CG+}} &\simeq H_+ + D \\ L_{\mathrm{IC}} &\simeq H + 2D = (H_+ - H_-) + 2D \quad . \end{aligned}$$

Here we neglect the zig–zag structure of the lightning channel and assume that D presents a meaningful average of its horizontal part: shorter discharges in that layer may occur as likely as longer, highly branched ones with an extent considerably longer than D. As shown in Tab. 2 this leads to a mean length of $L = 20 \pm 3$ km if the scale assumptions and the smaller Cb–cells are taken into account and $L = 35 \pm 8$ km if the larger dimensions of the EULINOX supercell are applied. This range corresponds surprisingly well to the mean flash length of 30 km derived by Théry et al. (2000) from the ITF data. However, as supercell storms are rare events in central Europe and can be expected on only a few days a year in Germany, we will go on assuming that the common mid–latitude thunderstorm is better represented by the arguments of the scale analysis. Therefore, in accordance with the conceptual picture of Fig. 2 we will use as a representative value of mean flash length:

$$\bar{L} \simeq 20 \text{ km} \quad .$$

For a more detailed distinction between the different flash types the reader is referred again to Tab. 2. To estimate $P(\mathrm{NO})$ we use the approach of Stith et al. (1999) which takes into account the density variation ($\rho \propto p/T$) of NO_X production in different altitude levels of the atmosphere:

$$\frac{dN_{\mathrm{NO}}}{dL} \simeq 5.69 \times 10^{25} \; \frac{p}{T} \; d^2 \; \bar{r}_{\mathrm{NO}} \quad \text{molec NO km}^{-1} \quad . \tag{1}$$

Here dN_{NO}/dL denotes the number of NO molecules per kilometer length L of the lightning channel, p and T are pressure and temperature, d is the diameter of the NO plume in meters, and $\bar{r}_{\mathrm{NO}}$ is the mean NO mixing ratio within the plume. Note that due to mass conservation of NO, $\bar{r}$ and d are dependent, i. e. $\bar{r}\, d^2 = \text{const}$ (cf. also Théry et al. (2000) for a discussion of this point). During EULINOX, local NO spikes up to 25 ppbv have been measured (Huntrieser et al., 2000). To account for the mean in–plume mixing ratio and plume diameter, we will use $d = 500$ m and $\bar{r} = 4$ ppbv.

3.4.1 LNO_X on a local scale

For the local estimate of $P(\mathrm{NO})$ we will consider the different properties of CG–, CG+, and IC lightning in the application of the Stith et al. (1999) formula. This affects flash length, pressure and temperature levels, and relative weight of the flash type. As shown in Tab. 3 we set the mean flash rate of the EULINOX storm between 17:00 and 19:00 UTC to 25 min^{-1} (Théry, 2000, this volume), resulting in a total of $N_{\mathrm{Total}} = 3000$ flashes. The variables R_ξ (here $\xi = \mathrm{IC},\ \mathrm{CG}-,\ \mathrm{CG}+$ denotes the flash type) are number ratios of the form $R_\xi = N_\xi/(N_{\mathrm{CG}} + N_{\mathrm{IC}})$ in which N_ξ denotes the number of flashes of a certain type. They represent mean values form the evaluation periods 1 and 2 from Théry (2000, this volume). Mean temperature and pressure in the table are flash length–weighted averages following the conceptual model of Fig. 2. The mean flash lengths for the EULINOX supercell follow from Tab. 2. Application of Eq. (1) leads to the tabulated values of molecules NO per kilometer flash.

So for each flash type ξ we compute its $P(\mathrm{NO})$ from the following equation in which $C = 23.26 \times 10^{-24}$ g(N) (molec NO)$^{-1}$, leading to

$$[P(\mathrm{NO})]_\xi \;=\; C \; N_\xi \; L_\xi \; \left[\frac{dN_{\mathrm{NO}}}{dL}\right]_\xi$$

$$P_{\mathrm{IC}} \;=\; 23.2 \text{ t(N)} \quad , \qquad P_{\mathrm{CG}-} \;=\; 2.2 \text{ t(N)} \quad , \qquad P_{\mathrm{CG}+} \;=\; 0.8 \text{ t(N)} \quad .$$

Table 3. Parameters of the 21 July EULINOX supercell storm (cf. Fig. 2, Tab. 2). Assuming a mean flash rate of 25 min^{-1} in the storm between 17:00 and 19:00 UTC a total of $N_{\mathrm{Total}} = 3000$ flashes follows.

	CG−	CG+	IC
$\bar{L}$ in km	26.5	29.5	43.0
R in %	11	4	85
N	330	120	2550
$\bar{p}$ in hPa	511	447	400
$\bar{T}$ in K	263	253	250
$\frac{dN_{\mathrm{NO}}/dL}{\mathrm{molec\,NO\,km}^{-1}}$	1.1×10^{25}	1.0×10^{25}	9.1×10^{24}

The total amount of nitrogen fixation for the 21 July EULINOX case is then $P(\mathrm{NO}) = 26.2$ t(N). This is in good agreement with the model analysis of Fehr (2000a, p. 78) who found $P(\mathrm{NO}) = 28.7$ t(N) in his mesoscale model case study of the supercell. Also, Théry et al. (2000) derived 80 t(N) within eight hours for the whole storm system of 21 July 1998. So all three completely different approaches indicate a nitrogen fixation of roughly 10 to 15 t(N) per hour for the supercellular storm. It should be emphasized here that while IC flashes are only slightly less effective in producing $\mathrm{NO_X}$ than CG flashes (cf. Tab. 3) they even produce the majority of the storm's total $\mathrm{NO_X}$.

3.4.2 $\mathrm{LNO_X}$ on a global scale

Following the EULINOX results of the preceding paragraph and Huntrieser et al. (2000), for the global estimate of $P(\mathrm{NO})$ we use one mean flash length $\bar{L} = 20$ km and assume that IC lightning is as effective in producing $\mathrm{NO_X}$ as CG lightning flashes. The approach is similar to the one presented above, but now we use a mean global flash rate (80 s^{-1}, a little lower than the usually assumed 100 s^{-1} according to Huntrieser et al. (2000)), and a mean NO production per kilometer flash length (8.75×10^{24} molecules) from Eq. (1). We also include physically sound variations to these mean values. With the intervals given in brackets and a conversion factor C to the unit $\mathrm{Tg(N)\,a}^{-1}$ this leads to

$$P(\mathrm{NO}) = C\,\bar{L}\,[50,100]\ \mathrm{fl\,s}^{-1}\ [4,15] \times 10^{24}\ \mathrm{molec\ NO\,km}^{-1}$$

$$P(\mathrm{NO}) = [2.9,22]\ \mathrm{Tg(N)\,a}^{-1} \quad , \qquad \bar{P}(\mathrm{NO}) = 10\ \mathrm{Tg(N)\,a}^{-1} \quad .$$

We see that the mean value of 10 $\mathrm{Tg(N)\,a}^{-1}$ is bracketed reasonably close. The interval found using our model approach is almost identical with that given by Huntrieser et al. (2000, this volume). However, their mean value of 3 $\mathrm{Tg(N)\,a}^{-1}$ lies near the lower end of our estimate. It must be noted, however, that Théry et al. (2000) derive a mean P(NO)= 22 $\mathrm{Tg(N)\,a}^{-1}$ from their detailed ITF analysis. Considering the large uncertainties involved in a global extrapolation and taking into account the simplicity of our proposed model we cannot give a tighter interval around the global nitrogen fixation due to thunderstorms. Instead the conceptual model, despite its simplicity, yields a good working hypothesis for future development of $\mathrm{LNO_X}$ parameterizations for mesoscale models.

4. Discussion

The results obtained yield an instructive view on the 21 July 1998 EULINOX supercell storm. Some theoretical predictions could already be corroborated with our combination of VHF interferometry and polarimetric Doppler radar measurements. The three–

dimensional information on cloud structure and lightning activity gathered by these two systems was extremely important for a successful evaluation within the mission objectives of the EULINOX project.

Combining ONERA's ITF data and DLR's radar measurements also provided some evidence for charge separation due to the riming graupel–ice crystal interaction mechanism within the updraft core of the growing thundercloud. Theoretical and experimental work (Williams, 1989; Williams et al., 1989; Saunders, 1993; Brooks et al., 1997; Stolzenburg & Marshall, 1998; MacGorman & Rust, 1998; Takahashi et al., 1999) had predicted this close relation between lightning and graupel, but only the three–dimensional overlay of radar and ITF data allowed for an analysis of the zones inside the cloud where discharges were more or less horizontally layered or formed structures vertically aligned downshear of the main updraft. In both cases most of the lightning discharges occurred in regions with graupel pellets.

As in similar investigations (Carey & Rutledge, 1998; Dye et al., 1999; Lang et al., 1999; Rison et al., 1999) the main point concerning the spatial extent of lightning activity was that intracloud lightning discharges can encompass the whole horizontal dimension of the cloud. In their detailed analysis of the ITF data Théry et al. (2000, this volume) quantifiy this impression by deriving a mean flash length of 30 km for the EULINOX storm. For the vertical structure of lightning activity our results are less unequivocal: in some parts of the cloud VHF signatures supporting the tripole model of thunderstorms appeared to be present, in other parts no evidence of a tripole structure could be detected. With Rust & Marshall (1996) we can conclude here that the real structure of thunderstorm is far more complex than the simple tripole concept, even though the physical processes leading to the tripole are likely to be present in parts of the thundercloud. Therefore the tripole model is most frequently applied in a conceptual context.

To make a step towards a development of lightning parameterizations derived from the EULINOX results we have proposed a simple model of lightning activity. Even with its highly idealized assumptions we were able to come quite close to other EULINOX results. For the main 2–hour period of the storm we derived a nitrogen fixation of 26.2 t(N). Fehr (2000a,b) used a completely different approach in a modeling case study of the 21 July supercell, but concludes with nearly the same value. Also Théry et al. (2000) found 80 t(N) for the whole lifetime of the EULINOX storm complex, i. e. 14:00–22:00 UTC, by evaluation of the ITF raw data. So all three different approaches lead to about 10 to 15 t(N) per hour for this storm. Despite the models simplicity and the general uncertainties involved with an extrapolation of an assumed average thunderstorm we also performed a bulk estimate of global annual nitrogen fixation by thunderstorms. The mean value of 10 $\mathrm{Tg(N)\,a^{-1}}$ and the interval of $[2.9, 22]$ $\mathrm{Tg(N)\,a^{-1}}$ are reasonable, but due to its simplicity our model definitely cannot be expected to give a smaller range. However, the fact that a reasonable global nitrogen fixation is computed from it seems to be a promising indicator that the model might become a basic part of future lightning parameterizations derived from the EULINOX results.

Finally, a puzzling feature remains to be addressed: the strong VHF activity near the freezing level within the supercell storm. On the one hand this would indicate that the lower (secondary) positive charge layer of the Cb–cloud was overwhelmingly active in this special case. Physical evidence for this assumption is given by Williams (1989) and also Shepherd et al. (1996) who observed strong electric fields and charges near the melting layer in the stratiform part of mesoscale convective systems. As these are even

larger than single supercell storms, the presence of strong electrical activity near the 0°C layer could probably turn out to be an indicator of storm severity in the future. On the other hand low–level negative leaders which were found in the data from the EULINOX supercell are likely to be even more prominent in VHF due to the higher air pressure at this low altitude (Lalande & Bondiou–Clergerie, 1997) and so to further enhance the VHF signatures of lightning activity there. However, the investigation here was focused on the higher levels inside the Cb–cloud and on bulk–statistics needed to evaluate the nitrogen fixation potential of the storm. For the upcoming analysis of other EULINOX days with different types and locations of storms, clarifying the processes that govern cloud electricity near the freezing level will present a fruitful and challenging task.

5. Conclusions

From the analysis of the radar and ITF data collected in the 21 July 1998 EULINOX supercell storm event we draw the following conclusions:

1. cloud microphysical aspects of thunderstorm electricity could effectively be studied with the combination of a polarimetric radar and a VHF lightning mapper,

2. in some parts of the Cb–cloud lightning flashes were initiated from certain height regions, resembling the upper positive charge center, the negative region around the –15°C altitude, and a lower positive charge layer near the freezing level,

3. these charge layers were not universally detectable inside the cloud, especially where strong convective motions dominate the Cb dynamics,

4. most VHF lightning signals were found in the regions of the Cb with large graupel pellets and small dry hail,

5. a simple model of lightning activity yielded a flash length range of $L = 35 \pm 8$ km for the special case of the EULINOX supercell.

6. according to our model the EULINOX supercell produced about 26 t(N) from 17:00–19:00 UTC, and a global estimate of $P(\mathrm{NO})$ was 10 $\mathrm{Tg(N)\,a^{-1}}$ with a range of $[2.9, 22]$ $\mathrm{Tg(N)\,a^{-1}}$.

Studying other cases of the EULINOX campaign will deepen the insight in the physics of lightning, not only within supercells, but for a variety of other storm types as well.

Acknowledgements

The authors are grateful to Thorsten Fehr for his critical proofreading and also to Ms M. Lewinsky for her careful typing of our manuscript.

Publications and References

Brooks, I. M., C. P. R. Saunders, R. P. Mitzeva, S. L. Peck, 1997: The effect on thunderstorm charging of the rate of rime accretion by graupel, *Atmos. Res.* **43**, 277–295.

Carey, L. D., S. A. Rutledge, 1998: Electrical and multiparameter radar observations of a severe hailstorm, *J. Geophys. Res.* **103**D, 13979–14000.

Defer, É., 1999: *Caractérisation et modélisation de l'activité électrique de nuages d'orage*, Ph. D. thesis, Univ. Paris VII, 233 pp.

Dye, J. E., T. Matejka, P. Laroche, É. Defer, G. Hubler, S. A. Rutledge, 1999: Lightning discharge locations relative to reflectivity and updraft / downdraft structures in a Colorado thunderstorm, *Proc. 11th Int. Conf. on Atmos. Electricity*, Huntsville, 530–533.

Fehr, T., 2000a: *Mesoskalige Modellierung der Produktion und des dreidimensionalen Transports von Stickoxiden in Gewittern*, Ph. D. thesis, Univ. Munich, 116 pp.

Fehr, T., 2000b: Study of lightning–induced NO$_X$ in a cloud–scale thunderstorm model, *EULINOX — final report*, European commission, Luxembourg, this volume.

Gallardo, L., V. Cooray, 1996: Could cloud–to–cloud discharges be as effective as cloud–to–ground discharges in producing NO$_X$?, *Tellus* **48**B, 641–651.

Höller, H., 1995: Radar–derived mass–concentrations of hydrometeors for cloud model retrievals, *Proc. 27th Conf. on Radar Meteorol.*, Vail, 453–454.

Höller, H., V. N. Bringi, J. Hubbert, M. Hagen, P. F. Meischner, 1994: Life cycle and precipitation formation in a hybrid–type hailstorm revealed by polarimetric and Doppler radar measurements, *J. Atmos. Sci.* **51**, 2500–2522.

Höller, H., U. Finke, H. Huntrieser, M. Hagen, C. Feigl, 1999a: Lightning–produced NO$_X$ (LINOX): Experimental design and case study results, *J. Geophys. Res.* **104**D, 13911–13922.

Höller, H., P. Laroche, M. Hagen, J. Seltmann, U. Finke, 1999b: Radar and lightning structures of thunderstorms during EULINOX, *Proc. 29th Conf. on Radar Meteorol.*, Montreal, 611–612.

Höller, H., H. Huntrieser, C. Feigl, C. Théry, P. Laroche, U. Finke, J. Seltmann, 2000: The severe storms of 21 July 1998 — Evolution and implications for NO$_X$ production, *EULINOX — final report*, European commission, Luxembourg, this volume.

Houze, R. A., 1993: *Cloud Dynamics*, Int. Geophys. Ser. Vol. **53**, Academic Press, San Diego, 570 pp.

Huntrieser, H., C. Feigl, H. Schlager, F. Schröder, C. Gerbig, P. van Velthoven, F. Flatøy, C. Théry, U. Schumann, 2000: Contribution of lightning–produced NO$_X$ to the European and global NO$_X$ budget: Results and estimates from airborne EULINOX measurements, *EULINOX — final report*, European commission, Luxembourg, this volume.

Lalande, P, A. Bondiou–Clergerie, 1997: Collection and analysis of available in–flight measurement of lightning strikes to aircraft. *Final report of Fulmen European Project on Analysis of Experimental data and models for upgraded lightning protection requirements*, DG VII, Transport Research and Technological Development Programs. Rep. Al–95–SC.204–RE / 210–D:1.

Lang, T. J., S. A. Rutledge, P. C. Kennedy, 1999: Combined dual–Doppler, multiparameter radar, and lightning observations of a severe convective storm, *Proc. 11th Int. Conf. on Atmos. Electricity*, Huntsville, 500–502.

Laroche, P., Defer, É., P. Blanchet, C. Théry, 1999: Evaluation of NO$_X$ produced by storms based on 3D VHF lightning mapping, *Proc. 11th Int. Conf. on Atmos. Electricity*, Huntsville, 656–659.

MacGorman, D. R., W. D. Rust, 1998: *The Electrical Nature of Storms*, Univ. Press, Oxford, 422 pp.

Price, C., D. Rind, 1992: A simple lightning parameterization for calculating global lightning distributions, *J. Geophys. Res.* **97**D, 9919–9933.

Price, C., D. Rind, 1993: What determines the cloud–to–ground fraction in thunderstorms?, *Geophys. Res. Lett.* **20**, 463–466.

Rison, W., R. Scott, R. J. Thomas, P. R. Krehbiel, T. Hamlin, J. Harlin, 1999: 3–dimensional lightning and dual–polarization observations of thunderstorms in central New Mexico, *Proc. 11th Int. Conf. on Atmos. Electricity*, Huntsville, 432–435.

Rust, W. D., T. C. Marshall, 1996: On abandoning the thunderstorm tripole–charge paradigm, *J. Geophys. Res.* **101**D, 23499–23504.

Saunders, C. P. R., 1993: A review of thunderstorm electrification processes, *J. Appl. Meteorol.* **32**, 642–655.

Shao, X.–M., P. R. Krehbiel, 1996: The spatial and temporal development of intracloud lightning, *J. Geophys. Res.* **101**D, 26641–26668.

Shepherd, T. R., W. D. Rust, T. C. Marshall, 1996: Electric fields and charges near 0°C in stratiform clouds, *Mon. Wea. Rev.* **124**, 919–938.

Solomon, R., C. Théry, É. Defer, A. Bondiou–Clergerie, 1999: Thunderstorm and lightning development: modeling and observations, *Proc. 11th Int. Conf. on Atmos. Electricity*, Huntsville, 335–338.

Stith, J., J. E. Dye, B. Ridley, P. Laroche, É. Defer, K. Baumann, G. Hübler, R. Zerr, M. Venticinque, 1999: NO signatures from lightning flashes, *J. Geophys. Res.* **104**D, 16081–16089.

Stolzenburg, M., T. C. Marshall, 1998: Charged precipitation and electric field in two thunderstorms, *J. Geophys. Res.* **103**D, 19777–19790.

Takahashi, T., T. Tajiri, Y. Sonoi, 1999: Charges on graupel and snow crystals and the electrical structure of winter thunderstorms, *J. Atmos. Sci.* **56**, 1561–1578.

Théry, C., 2000: Evaluation of LPATS data using VHF interferometric observations of lightning flashes during the EULINOX experiment, *EULINOX — final report*, European commission, Luxembourg, this volume.

Théry, C., P. Laroche, P. Blanchet, 2000: Lightning activity during EULINOX and estimation of NO_X production by flashes, *EULINOX — final report*, European commission, Luxembourg, this volume.

Williams, E. R., 1989: The tripole structure of thunderstorms, *J. Geophys. Res.* **94**D, 13151–13167.

Williams, E. R., M. E. Weber, R. E. Orville, 1989: The relationship between lightning type and convective state of thunderclouds, *J. Geophys. Res.* **94**D, 13213–13220.